DOI: 10.61782/fa.2023.0727

forum acusticum 2023

FLANKING SOUND TRANSMISSION THROUGH CROSS-LAMINATED TIMBER JUNCTIONS WITH ELASTIC INTERLAYERS: PREDICTION MODEL AND VALIDATION

Stijn Moons[1*] **Wannes Stalmans**[1] **Cédric Van hoorickx**[1]
Reinhilde Lanoye[2] **Edwin Reynders**[1]
[1] Department of Civil Engineering, Faculty of Engineering Science, KU Leuven, Belgium
[2] CDM Stravitec, Reutenbeek 9/11, 3090 Overijse, Belgium

ABSTRACT

Cross-laminated timber (CLT) has experienced significant growth in popularity due to among others high structural stiffness and low weight. However, these two properties lead to potentially poor sound insulation. In order to suppress flanking sound, where vibrational energy is transmitted from one wall or floor to another through their common junction, elastic interlayers are typically employed, but the potential improvements are not straightforward to predict. In the present work, the vibration reduction index K_{ij} for wave transmission between two connected elements i and j is predicted based on analytical wave theory for semi-infinite thin homogeneous orthotropic plates. The junctions can be rigid or they can contain elastic interlayers modeled as distributed springs or flexible waveguides. The proposed methodology is validated with on-site experiments on a T- junction consisting of CLT-panels with a resilient interlayer. Static equivalence is used to obtain the model input parameters. The model predictions are in reasonable agreement with the experimental results for the entire frequency range, especially for the flexible interlayer models. The differences between the equivalent isotropic and orthotropic plate model predictions remain small.

Keywords: *cross-laminated timber, flanking sound, elastic interlayers.*

**Corresponding author*: *stijn.moons@kuleuven.be.*

1. INTRODUCTION

In flanking sound transmission, vibrational energy is transmitted from one structural element (e.g. wall or plate) to another through their common junction. In cross-laminated timber (CLT) structures this often contributes significantly to the overall sound transmission between rooms. This may result in an unsatisfactory acoustic comfort level. In order to suppress the transmission of flanking sound, elastic interlayers are sometimes implemented in structural junctions between walls and/or floors. In this report, an analytical prediction model for flanking transmission using a wave approach is presented. Section 2 describes the general modeling approach to determine the transmission coefficients and vibration reduction indices. In Section 3 this methodology is specified for directly connected orthotropic plates. Section 4 describes the expansion of this approach to continuous elastic interlayers. In Section 5 a validation example of a CLT-structure is treated.

2. METHODOLOGY

The system of interest is a junction consisting of n directly connected plates with each an inclination θ_j relative to an arbitrary plate for which $j = 1$. The overall system is illustrated in Figure 1. The general aim of the prediction model is to determine the transmission coefficients τ_{ij}^{st} between an incident wave type s in plate i and transmitted wave type t in plate j. This is the ratio of the power transmitted to a receiver plate j from the junction to the power impinging on the junction from the source plate i. This coefficient is required for calculating engineering quantities such as the vibration

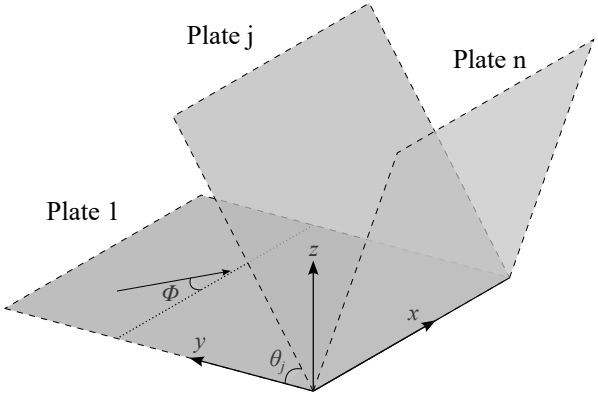

Figure 1. General plate system.

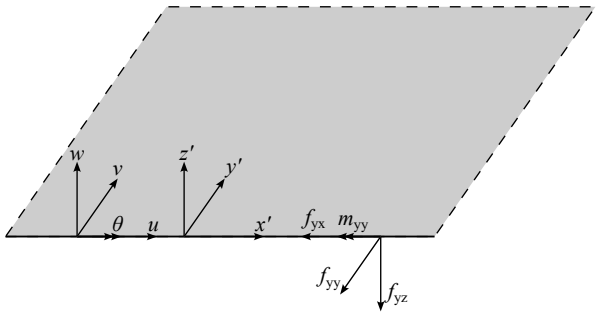

Figure 2. Forces and displacements at a plate edge.

reduction index K_{ij}. The developments start from a wave approach framework as introduced in [1]. Each plate is considered to be a thin homogeneous Kirchhoff-Love plate [2] with an infinite junction length. The wave transmission between the plates entails an exchange of vibrational energy between *subsystems* of source plate i and receiver plate j, respectively wave types s and t. In this assessment, three plane wave types are considered for each plate: out-of-plane bending waves B, in-plane *fast* waves F and in-plane *slow* waves S. Depending on the propagation angle ϕ, the latter two types are a combination of quasi-longitudinal and shear wave motion. The in-plane and out-of-plane motion are taken to be completely uncoupled.

An incident plane wave of type s in the source plate i with a given dependence on the angular frequency ω and wavenumber k_x in the x-direction which is parallel to the junction, impinges on the junction at an angle ϕ_i. This elicits a response in the form of reflected and transmitted plane waves from the junction to every receiver plate j for any potential wave type t. Due to the compatibility at the junction these waves have an imposed dependency on ω and k_x as well. This means the x-component of each wavenumber is identical for all plates and chosen freely for the incident wave. Similarly, the amplitude is up to choice. The angle of incidence ϕ_i depends on k_x with $\tan\left(\phi_i^s\right) = \frac{k^s_{\mathrm{y},i}}{k^s_{\mathrm{x},i}}$. Based on this imposed dependency, the form of the displacements u, v, w and θ on each plate edge can be derived. The incident, reflected and transmitted waves at the junction will also result in forces per unit length or *tractions* f_yx, f_yy and f_yz and a moment m_yy in every receiver plate. The tractions along with the displacements and rotation at the neutral plane of the plates in the local coordinate system are illustrated in Figure 2. The plate edge deformations $\mathbf{u}_j$ and tractions $\mathbf{F}_j$ for a plate j consist of contributions due to the outgoing transmitted and reflected waves at the junction $\mathbf{u}_{\mathrm{out},j}$ and the incident wave $\mathbf{u}_\mathrm{inc}$:

$$\mathbf{u}_j = \mathbf{u}_{\mathrm{out},j} + \mathbf{u}_\mathrm{inc}, \tag{1}$$

$$\mathbf{F}_j = \mathbf{F}_{\mathrm{out},j} + \mathbf{F}_\mathrm{inc}. \tag{2}$$

For any plate other than the source plate there is no incident wave, so $\mathbf{u}_\mathrm{inc} = 0$ and $\mathbf{F}_\mathrm{inc} = 0$. The tractions $\mathbf{F}_{\mathrm{out},j}$ are related to the edge displacements of the plate $\mathbf{u}_{\mathrm{out},j}$ in the local coordinate system (x', y', z') by a block diagonal stiffness matrix $\mathbf{D} \in \mathbb{C}^{4x4}$ consisting of two matrices $\mathbf{D}_\mathrm{IP}$ and $\mathbf{D}_\mathrm{OOP} \in \mathbb{C}^{2x2}$ respectively related to the in-plane (IP) and out-of-plane (OOP) components. The stiffness matrices are function of the imposed wavenumber k_x:

$$\underbrace{\begin{bmatrix} f_{yx} \\ f_{yy} \\ f_{yz} \\ m_{yy} \end{bmatrix}}_{:=\mathbf{F}_{\mathrm{out},j}} = \underbrace{\begin{bmatrix} \mathbf{D}_\mathrm{IP}\left(k_\mathrm{x}\right) & \mathbf{0} \\ \mathbf{0} & \mathbf{D}_\mathrm{OOP}\left(k_\mathrm{x}\right) \end{bmatrix}}_{\mathbf{D}_j(k_\mathrm{x})} \underbrace{\begin{bmatrix} u\left(y'=0\right) \\ v\left(y'=0\right) \\ w\left(y'=0\right) \\ \theta\left(y'=0\right) \end{bmatrix}}_{\mathbf{u}_{\mathrm{out},j}}. \tag{3}$$

In a first step, the stiffness matrices $\mathbf{D}_j$ are constructed for all plates for a given junction displacement and frequency. Secondly, the tractions $\mathbf{F}_\mathrm{inc}$ due to the incident wave are determined from the same stiffness relations for a chosen $\mathbf{u}_\mathrm{inc}$. Then the force and moment equilibrium and deformation placement compatibility conditions are evaluated at the junction in the global coordinate system such that

$$\Sigma_{j=1}^{n} \mathbf{D}_j \mathbf{u}_j = \mathbf{f}_\mathrm{inc} \quad \text{where} \quad \mathbf{f}_\mathrm{inc} = \mathbf{D}_i \mathbf{u}_\mathrm{inc} - \mathbf{F}_\mathrm{inc}. \tag{4}$$

This system is solved for the displacements $\mathbf{u}_j$. The edge displacements of each plate can be determined from the displacement compatibility conditions of the connected plate. The incident and transmitted intensity to plate j in the local y'-direction is subsequently computed from the tractions and edge deformations of each plate for a given wave type as in [3, p. 34]:

$$I_{\mathrm{y},j} := \frac{1}{2}\mathrm{Re}\left(\mathbf{F}_j \dot{\mathbf{u}}_j^*\right), \tag{5}$$

with $\dot{\mathbf{u}}_j^*$ the complex conjugate of the time derivative of the displacement. Finally, the transmission coefficient for an incident wave of type s in a source plate i and transmitted wave of type t in receiver plate j can be calculated:

$$\tau_{ij}^{st}\left(\omega, \phi_i\right) := \frac{I_{\mathrm{y},j}^t}{I_{\mathrm{y},i}^s}. \tag{6}$$

For practical purposes it is more relevant to use an angle-independent *diffuse* transmission coefficient:

$$\overline{\tau}_{ij}^{st}\left(\omega\right) := \frac{\frac{1}{2}\int_0^{\pi/2} I_{\mathrm{y},j}^t D_{\mathrm{sw},i}\left(\phi_i\right)\mathrm{d}\phi_i}{\frac{1}{2}\int_0^{\pi/2} I_{\mathrm{y},i}^s D_{\mathrm{tw},i}\left(\phi_i\right)\mathrm{d}\phi_i}, \tag{7}$$

with a direction-dependent weighting factor $D_{\mathrm{w}}\left(\phi\right)$ which accounts for the fact that waves in different directions carry the same energy, so they have different intensity if the group speed is directionally dependent [4, p. 69]. The vibration reduction index K_{ij} of connected elements i and j follows from the transmission coefficients:

$$K_{ij} := \frac{\mathrm{TL}_{ij}^{\mathrm{BB}} + \mathrm{TL}_{ji}^{\mathrm{BB}}}{2} + 5\log\left(\frac{\sqrt{f_{\mathrm{c},i} f_{\mathrm{c},j}}}{f_{\mathrm{ref}}}\right), \tag{8}$$

with

$$\mathrm{TL}_{ij}^{\mathrm{BB}} = -10\log\left(\overline{\tau}_{ij}^{\mathrm{BB}}\right), \tag{9}$$

for a reference frequency $f_{\mathrm{ref}} = 1000\,\mathrm{Hz}$ and critical frequencies $f_{\mathrm{c},i/j}$.

3. PLATE MODELS

The procedure described in the previous section is adapted for undamped orthotropic plates with a constant thickness t and mass density ρ. The local coordinate system of the plate is oriented along the principal material directions [5]. There are four independent elastic constants: the Young's moduli E_{x}, E_{y}, Poisson coefficient ν_{xy} and shear modulus G_{xy}. The other Poisson coefficient follows from the symmetry condition:

$$\nu_{\mathrm{xy}} E_{\mathrm{y}} = \nu_{\mathrm{yx}} E_{\mathrm{x}}. \tag{10}$$

Isotropic plates are a special case of the orthotropic plate model with

$$E = E_{\mathrm{x}} = E_{\mathrm{y}}, \quad \nu = \nu_{\mathrm{xy}} = \nu_{\mathrm{yx}} \text{ and } G = \frac{E}{2\left(1+\nu\right)}. \tag{11}$$

The deformation of the plate is approximated as a superposition of in-plane deformation under plane stress conditions for the local $x'y'$-plane and bending deformation satisfying Kirchhoff's assumptions with the following governing equations of motion:

$$E'_{\mathrm{x}}\frac{\partial^2 u}{\partial x'^2} + G_{\mathrm{xy}}\frac{\partial^2 u}{\partial y'^2} + A\frac{\partial^2 v}{\partial x'\partial y'} = \rho\frac{\partial^2 u}{\partial t^2}, \tag{12}$$

$$E'_{\mathrm{y}}\frac{\partial^2 v}{\partial y'^2} + G_{\mathrm{xy}}\frac{\partial^2 v}{\partial x'^2} + A\frac{\partial^2 u}{\partial x'\partial y'} = \rho\frac{\partial^2 v}{\partial t^2}, \tag{13}$$

$$B_x\frac{\partial^4 w}{\partial x'^4} + 2B_{\mathrm{xy}}\frac{\partial^4 w}{\partial x'^2\partial y'^2} + B_{\mathrm{y}}\frac{\partial^4 w}{\partial y'^4} + \rho t\frac{\partial^2 w}{\partial t^2} = 0, \tag{14}$$

with

$$E'_{\mathrm{x}} := \frac{E_{\mathrm{x}}}{1-\nu_{\mathrm{xy}}\nu_{\mathrm{yx}}}, \quad B_{\mathrm{x}} := \frac{E_{\mathrm{x}} t^3}{12\left(1-\nu_{\mathrm{xy}}\nu_{\mathrm{yx}}\right)}, \tag{15}$$

$$E'_{\mathrm{y}} := \frac{E_{\mathrm{y}}}{1-\nu_{\mathrm{xy}}\nu_{\mathrm{yx}}}, \quad B_{\mathrm{y}} := \frac{E_{\mathrm{y}} t^3}{12\left(1-\nu_{\mathrm{xy}}\nu_{\mathrm{yx}}\right)}, \tag{16}$$

$$A := \nu_{\mathrm{xy}} E'_{\mathrm{y}} + G_{\mathrm{xy}}, \quad B_{\mathrm{xy}} := \nu_{\mathrm{xy}} B_{\mathrm{y}} + 2\frac{G_{\mathrm{xy}} t^3}{12}. \tag{17}$$

Compatibility at the junction requires the same dependency for the deformations of each plate:

$$\mathbf{u}\left(x, y, t\right) = \alpha_j \mathrm{e}^{-\mathrm{i}k_{\mathrm{x}}x'}\mathrm{e}^{-\mathrm{i}k_{ty}y'}\mathrm{e}^{\mathrm{i}\omega t}, \tag{18}$$

The in-plane displacements are assumed to differ only by an amplitude ratio V of v to u. Substitution of equation (18) into the equations of motion results in a bi-quadratic equation for both out-of-plane and in-plane motion in function of their respective wavenumbers in the y'-direction k_{ty} for a transmitted wave type t. Two solutions of k_{ty} for both in-plane and out-of-plane motion are selected for the condition that transmitted waves decay or propagate in the positive y'-direction. Similarly, the amplitude ratios for two different fast or slow in-plane waves $V_{\mathrm{F/S}}$ are determined. The stiffness matrix $\mathbf{D}\left(k_{\mathrm{x}}\right)$ consists of decoupled in-plane and out-of-plane components as in equation (3):

$$\mathbf{D}_{\mathrm{IP}}\left(k_{\mathrm{x}}\right) = \begin{bmatrix} D_{11} & D_{12} \\ D_{21} & D_{22} \end{bmatrix}, \tag{19}$$

$$\mathbf{D}_{\mathrm{OOP}}\left(k_{\mathrm{x}}\right)=\frac{B_{\mathrm{y}}}{k_{\mathrm{B1y}}-k_{\mathrm{B2y}}}\begin{bmatrix}D_{33} & D_{34}\\ D_{43} & D_{44}\end{bmatrix}, \tag{20}$$

with

$$D_{11}=G_{\mathrm{xy}}t\left(\frac{\mathrm{i}V_{\mathrm{S}}k_{\mathrm{Fy}}-\mathrm{i}V_{\mathrm{F}}k_{\mathrm{Sy}}}{V_{\mathrm{F}}-V_{\mathrm{S}}}\right), \tag{21}$$

$$D_{12}=G_{\mathrm{xy}}t\left(\frac{\mathrm{i}k_{\mathrm{Sy}}-\mathrm{i}k_{\mathrm{Fy}}}{V_{\mathrm{F}}-V_{\mathrm{S}}}-\mathrm{i}k_{\mathrm{x}}\right), \tag{22}$$

$$D_{21}=E'_{\mathrm{y}}t\left(\frac{V_{\mathrm{F}}V_{\mathrm{S}}\left(\mathrm{i}k_{\mathrm{Fy}}-\mathrm{i}k_{\mathrm{Sy}}\right)}{V_{\mathrm{F}}-V_{\mathrm{S}}}\right)-\mathrm{i}k_{\mathrm{x}}\nu_{\mathrm{xy}}, \tag{23}$$

$$D_{22}=E'_{\mathrm{y}}t\left(\frac{\mathrm{i}V_{\mathrm{S}}k_{\mathrm{Sy}}-\mathrm{i}V_{\mathrm{F}}k_{\mathrm{Fy}}}{V_{\mathrm{F}}-V_{\mathrm{S}}}\right), \tag{24}$$

$$D_{33}=\mathrm{i}k_{\mathrm{B1y}}^{3}k_{\mathrm{B2y}}-\mathrm{i}k_{\mathrm{B2y}}^{3}k_{\mathrm{B1y}}, \tag{25}$$

$$\begin{aligned}D_{34}=&k_{\mathrm{B1y}}^{3}-k_{\mathrm{B1y}}^{3}+\nu_{\mathrm{xy}}\left(k_{\mathrm{B1y}}-k_{\mathrm{B2y}}\right)k_{\mathrm{x}}^{2}\\&+\frac{4G_{\mathrm{xy}}}{E_{\mathrm{y}}}\left(1-\nu_{\mathrm{xy}}\nu_{\mathrm{yx}}\right)\left(k_{\mathrm{B1y}}-k_{\mathrm{B2y}}\right)k_{\mathrm{x}}^{2},\end{aligned} \tag{26}$$

$$D_{43}=k_{\mathrm{B1y}}^{2}k_{\mathrm{B2y}}-k_{\mathrm{B2y}}^{2}k_{\mathrm{B1y}}-\nu_{\mathrm{xy}}\left(k_{\mathrm{B1y}}-k_{\mathrm{B2y}}\right), \tag{27}$$

$$D_{44}=\mathrm{i}k_{\mathrm{B2y}}^{2}-\mathrm{i}k_{\mathrm{B1y}}^{2}. \tag{28}$$

The vibration reduction indices are found by applying the procedure presented in the previous section.

4. INTERLAYER MODELS

In order to suppress flanking transmission sometimes resilient strips are employed. These interlayers exert additional tractions $\mathbf{F}_{\mathrm{lay}}=\left[\mathbf{F}_{\mathrm{lay},1},\mathbf{F}_{\mathrm{lay},2}\right]^{\mathbf{T}}$ on both the plate they are connected to (1) and the junction (2) as in Figure 3. These tractions are related to the deformations at the endplanes of the interlayer $\mathbf{u}_{\mathrm{lay}}=\left[\mathbf{u}_{\mathrm{lay},1},\mathbf{u}_{\mathrm{lay},2}\right]^{\mathbf{T}}$ by a stiffness matrix $\mathbf{D}_{\mathrm{lay}}$ such that

$$\mathbf{F}_{\mathrm{lay}}=\mathbf{D}_{\mathrm{lay}}\mathbf{u}_{\mathrm{lay}}. \tag{29}$$

The force and moment equilibrium is evaluated at both ends of the interlayer in function of the deformations on the endfaces of the layer. From these deformations, K_{ij} can be obtained with the procedure from Section 2. The interlayer modeling procedure consists of constructing the interlayer stiffness matrix $\mathbf{D}_{\mathrm{lay}}$. For readibility, the subscript lay is dropped in further equations. The resilient interlayer is considered as an isotropic material with an infinite x'-dimension and finite y'-dimension. Unlike for the plates, damping is included by means of a complex Young's modulus $E\left(1+\mathrm{i}\eta\right)$ with an internal loss factor η. The position of the layer relative to the junction line is

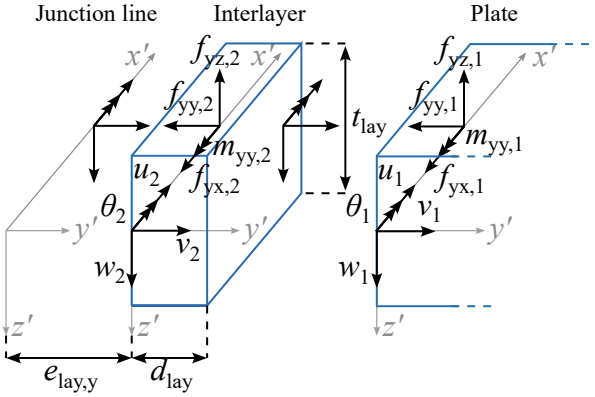

Figure 3. Exploded view of the plate/interlayer system.

characterized by the offset e_{y}.

In what follows, three candidate interlayer models are considered. In a first model the interlayer is a thin isotropic plate. The interlayer stiffness matrix is analogous to that of the previous section with the exception that the layer is a waveguide instead of a halfspace, such that waves can propagate in both the positive and negative y'-direction. A second model satisfies the assumptions from Mees and Vermeir [6]. The in- and out-of-plane wave motion are also completely uncoupled here. In order to determine u and v, plane strain conditions are assumed for the in-plane deformations, which is valid for strips with a large thickness t compared to the width d and rigidly attached endplanes. The bending stiffness is considered negligible such that the out-of-plane deformation w is purely governed by shear. The cross-sectional rotation θ is taken to be independent from the out-of-plane translation. It is instead determined by quasi-longitudinal in-plane wave motion of infinitesimal layers in the z'-direction which deform independently from each other. These assumptions lead to the following relations between tractions and deformations:

$$f_{\mathrm{yx}}=\frac{Et}{2\left(1+\nu\right)}\left(\frac{\partial u}{\partial y'}+\frac{\partial v}{\partial x'}\right), \tag{30}$$

$$f_{\mathrm{yy}}=\frac{E\left(1-\nu\right)t}{\left(1+\nu\right)\left(1-2\nu\right)}\left(\frac{\nu}{1-\nu}\frac{\partial u}{\partial x'}+\frac{\partial v}{\partial y'}\right), \tag{31}$$

$$f_{\mathrm{yz}}=\frac{Et}{2\left(1+\nu\right)}\frac{\partial w}{\partial y'}, \tag{32}$$

$$m_{\mathrm{yy}}=\frac{Et^{3}\left(1-\nu\right)}{12\left(1+\nu\right)\left(1-2\nu\right)}\frac{\partial\theta}{\partial y'}. \tag{33}$$

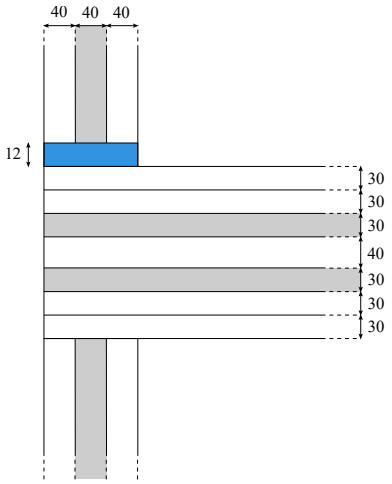

Figure 4. Layer geometry of the CLT-panels in the T-junction. White and grey layers have grain directions respectively perpendicular and parallel to the junction. Dimensions are in mm.

In the third model the interlayer is not a waveguide, but a set of spatially distributed springs along the x'-axis with no wave propagation in the interlayer in the x'-direction [6]. The other assumptions of the second model are still valid. The springs are in static equilibrium which means the tractions on both ends will be equal in magnitude with an opposite sign in function of the endplane deformations, resulting in

$$f_{\mathrm{yx}} = \frac{Et}{2\,(1+\nu)}\,\frac{u_1 - u_2}{d}, \tag{34}$$

$$f_{\mathrm{yy}} = \frac{Et\,(1-\nu)}{(1+\nu)\,(1-2\nu)}\,\frac{v_1 - v_2}{d}, \tag{35}$$

$$f_{\mathrm{yz}} = \frac{Et}{2\,(1+\nu)}\,\frac{w_1 - w_2}{d}, \tag{36}$$

$$m_{\mathrm{yy}} = \frac{Et^3\,(1-\nu)}{12\,(1+\nu)\,(1-2\nu)}\,\frac{\theta_1 - \theta_2}{d}. \tag{37}$$

5. APPLICATION

In situ experiments are carried out on a T-junction consisting of cross-laminated timber elements with a resilient polyurethane foam strip as illustrated in Figure 4. The experiments are conducted according to the international standard ISO 10848 [7] with transient hammer excitation and accelerometer measurements. The timber layers in the panels are of strength class C24. The nominal timber

Table 1. Equivalent elastic orthotropic constants

Element	E_{x}[MPa]	E_{y}[MPa]	G[MPa]	ν_{xy}[-]	ν_{yx}[-]
Floor	3561	8877	690	0.019	0.047
Walls	4270	8169	690	0.021	0.040

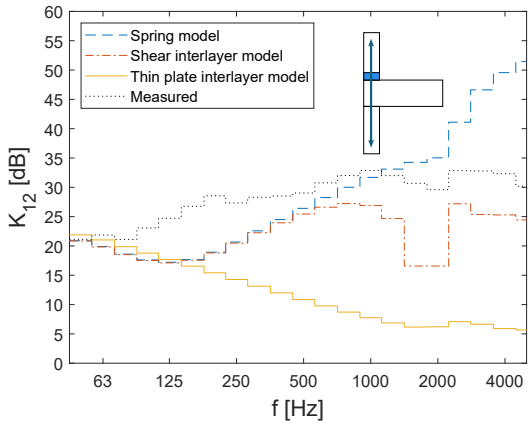

Figure 5. Upper wall-lower wall vibration reduction index for different interlayer models.

material properties are: $\rho = 420\,\mathrm{kg/m^3}$, $\nu_{\mathrm{yx}} = 0.4541$, $E_{\mathrm{x}} = 370\,\mathrm{MPa}$, $E_{\mathrm{y}} = 12\,\mathrm{GPa}$ and $G = 690\,\mathrm{MPa}$, in which x and y respectively denote the weak and strong principal direction [8, 9]. The interlayer properties are $E = 3.15\,\mathrm{MPa}$, $\nu = 0.4235$, $\rho = 585.7\,\mathrm{kg/m^3}$ and $\eta = 6.81\,\%$, as determined by CDM Stravitec. An interlayer offset $e_{\mathrm{lay,y}}$ of the half floor thickness is assumed. The elastic properties of an equivalent homogeneous plate are deduced by considering the tractions of the full equivalent cross-section equal to the sum of the tractions of each individual layer, assuming the layers are perfectly glued together. The elastic properties of this equivalent plate are the model input parameters, as in Table 1. The vibration reduction index K_{ij} for each transmission path ij is averaged for the 1/3 octave bands of 50 up to 5000 Hz. Figures 5, 6 and 7 show the predicted values for the three transmission paths for each interlayer model alongside the measured values.

It is clear that despite the identical plate models the predicted results differ greatly due to the varying nature of the interlayer models. Good estimates for interlayer material properties and mechanical behavior are therefore essential to the viability of the predictions as

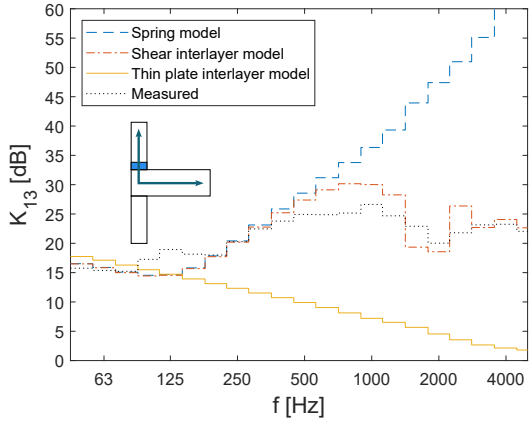

Figure 6. Upper wall-floor vibration reduction index for different interlayer models.

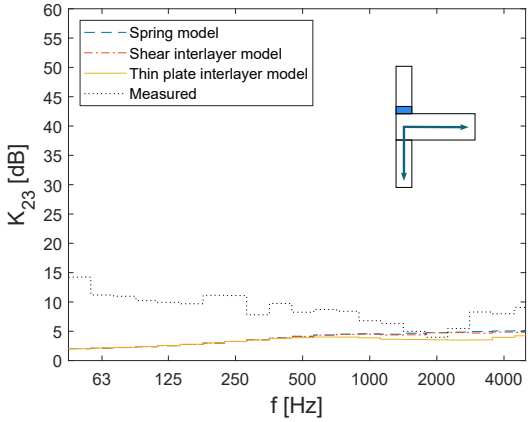

Figure 7. Lower wall-floor vibration reduction index for different interlayer models.

inaccuracies can result in large variations. The thin plate interlayer model predicts a different overall trend for K_{ij} than the other approaches and measured values with the exception of transmission path 2-3 which does not include the elastic strip. This is not surprising considering this path can be considered as a rigid L-junction due to the decoupling from the upper wall by the interlayer in each prediction. The model errors exceed even 20 dB for 5000 Hz. It can be concluded that this model is not appropriate for the prediction of resilient interlayer behavior.

The shear interlayer model and its simplified version with springs predict nearly identical results for the low frequency range up to approximately 200 Hz. The behavior at higher frequencies is different due to the frequency dependence of the shear interlayer model, resulting in resonance and anti-resonance dips or peaks instead of the steady rise predicted by the spring model. These phenomena occur when

$$\text{Resonance:} \quad d_{\text{lay}} = \frac{n\lambda_{\text{S,lay}}}{2}, \tag{38}$$

$$\text{Anti-resonance:} \quad d_{\text{lay}} = (2n+1)\,\frac{\lambda_{\text{S,lay}}}{4}, \tag{39}$$

with $\lambda_{\text{S,lay}}$ the shear wavelength of the interlayer and n a natural number. A shear resonance dip is visible in the band of 2000 Hz as well as an anti-resonance peak in the band of 2500 Hz for the transmission paths which include the resilient strip. Resonances at higher frequencies are not as clearly visible in a 1/3 octave analysis. This can also be observed in the experimental data, albeit less pronounced than predicted. The transverse bending and shear impedances of the source plate $Z_{\text{B},i}$ and interlayer $Z_{\text{S,lay}}$ are respectively

$$Z_{\text{B},i} := \rho_i t_i c_{\text{B},i}, \tag{40}$$

$$Z_{\text{S,lay}} := \frac{E_{\text{lay}} t_{\text{lay}}}{2\,(1+\nu_{\text{lay}})\,d_{\text{lay}}\omega}. \tag{41}$$

for a bending wavespeed in the source plate $c_{\text{B},i}$. These impedances match approximately at 125 Hz, resulting in a local minimum for the vibration reduction [10]. The measured values do not show this effect.

With the exception of the thin plate interlayer model, each model has reasonably accurate predictions in the low- and mid-frequency range up to 1000 Hz with deviations generally beneath 10 dB. The spring model overestimates the vibration reduction in the high frequency range due to the absence of resonances. Subsequently, the shear interlayer model is the most accurate in this range with deviations generally beneath 10 dB with the exception of the first resonance dip with an error of 14.1 dB. For transmission path 1-3, deviations remain below 5 dB for the entire frequency range. For path 2-3 the predictions are very accurate in the high-frequency range, but deviate significantly from the measured values in the low-frequency range. The overall deviation from the measurements however generally remains beneath 10 dB for every model which is similar to the other

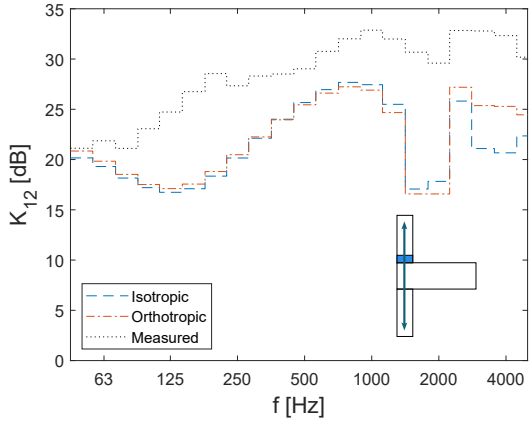

Figure 8. Upper wall-lower wall vibration reduction index for a shear interlayer model.

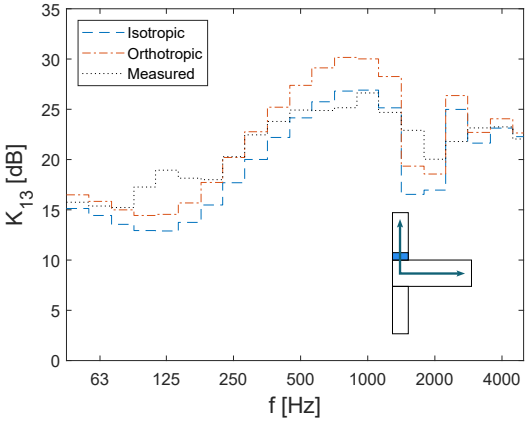

Figure 9. Upper wall-floor vibration reduction index for a shear interlayer model.

transmission paths.

In a further simplification, the CLT-panels are considered as isotropic plates with equivalent elastic constants: $E = \sqrt{E_x E_y}$ and $\nu = \sqrt{\nu_{xy}\nu_{yx}}$. Figures 8, 9 and 10 show a comparison of these predictions. The predictions of both isotropic and orthotropic plate models are very similar for every transmission path with differences generally below 5 dB. For transmission paths 1-2 and 2-3 these differences are even negligible with the exception of frequencies above 2000 Hz. This is not surprising as the equivalent Young's moduli in Table 1 differ with a factor less than three, which implies the material is *nearly* isotropic with these parameters. There is no clear indication that either plate model is more accurate than the other as these models relies heavily on the assumed equivalent material parameters. It can however be concluded that an isotropic equivalent model can deliver sufficiently accurate results for a representative choice of elastic parameters. This was also observed by Bosmans et al. for orthotropic L-junctions [5]. The chosen modeling approach for the resilient layer dominates over the choice between plate isotropy or orthotropy.

The model predictions are based on multiple assumptions which can decrease their accuracy. The assumption of a thin plate is not valid for a wavelength in the same order of magnitude as the plate thickness or smaller. At high frequencies, this is often the case for the transmitted bending waves in the CLT-panels. For example, in the isotropic equivalent model the wall thickness is a quarter of its bending wavelength for frequencies above 3500 Hz while for the floor this is already the case for 2000 Hz. The assumptions of infinite plate dimensions and diffuse fields in the plates are also not necessarily valid. It is not clear to what extent each individual assumption contributes to the total model error, especially in the case of the interlayer modeling approaches which can differ greatly. The validity of the models for varying junction set-ups and material properties should be evaluated with more extensive testing.

6. CONCLUSION

In this study a prediction model for flanking sound transmission using the wave approach has been described and validated using experimental results for a CLT structure. The proposed models provide moderately accurate predictions for the vibration reduction index K_{ij} in the case of both isotropic and orthotropic plate inputs with an elastic interlayer. The shear interlayer model is the most accurate representation of resilient strips throughout the entire frequency range from 50 to 5000 Hz while the less computionally intensive spring model is sufficiently accurate at least in the low and middle frequency range up to 1000 Hz. There is no significant difference between the orthotropic and isotropic equivalent models for the panels as long as the equivalent material properties are chosen carefully. The assumptions made for either the plates or the interlayer such as the infinite dimensions and thin na-

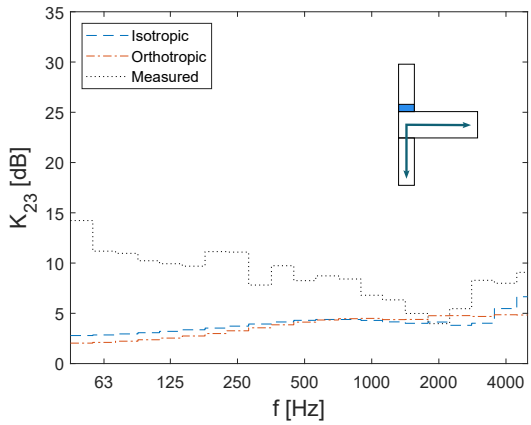

Figure 10. Lower wall-floor vibration reduction index for a shear interlayer model.

ture result in potential inaccuracies. Further confirmation by additional validation is necessary.

7. ACKNOWLEDGMENTS

The research is funded by a FLOF fellowship from the KU Leuven Department of Civil Engineering. The ability to perform on-site experiments was granted by CLT-S. Material properties of cross-laminated timber elements and resilient strips were provided by CLT-S and CDM Stravitec.

8. REFERENCES

[1] R. Langley and K. Heron, "Elastic wave transmission through plate/beam junctions," *Journal of Sound and Vibration*, vol. 143, no. 2, pp. 241–253, 1990.

[2] A. Love, "XVI. The small free vibrations and deformation of a thin elastic shell," *Philosophical Transactions of the Royal Society of London*, vol. 179, pp. 491–546, 1888.

[3] J. Rindel, *Sound insulation in buildings*. Boca Raton, FL: CRC Press, 2018.

[4] R. Lyon and R. DeJong, *Theory and application of statistical energy analysis*. Newton, MA: Butterworth-Heinemann, second ed., 1995.

[5] I. Bosmans, P. Mees, and G. Vermeir, "Structure-borne sound transmission between thin orthotropic plates: analytical solutions," *Journal of Sound and Vibration*, vol. 191, no. 1, pp. 75–90, 1996.

[6] P. Mees and G. Vermeir, "Structure-borne sound transmission at elastically connected plates," *Journal of Sound and Vibration*, vol. 166, no. 1, pp. 55–76, 1993.

[7] International Organization for Standardization, "Acoustics-laboratory and field measurement of flanking transmission for airborne, impact and building service equipment between adjoining rooms-part 1:frame document," Standard ISO/FDIS 10848-1:2017, International Organization for Standardization, Geneva, Switzerland, 2017.

[8] Stora Enso, "CLT by Stora Enso: Stifness matrix," tech. rep., Stora Enso, Helsinki, Finland, 2019.

[9] Austrian Institute of Construction Engineering, "European technical assessment eta-14/0349," Technical assessment ETA-14/0349, Austrian Institute of Construction Engineering, Vienna, Austria, 2020.

[10] R. Leung and R. Pinnington, "Wave propagation through right-angled joints with compliance-flexural incident wave," *Journal of Sound and Vibration*, vol. 142, no. 1, p. 31–46, 1990.